Essential Roles of a Dynamic Loop in the Catalysis of 6-Hydroxymethyl-7,8-dihydropterin Pyrophosphokinase†

Jaroslaw Blaszczyk,‡ Yue Li,§ Yan Wu,§ Genbin Shi,§,|| Xinhua Ji,*,‡ and Honggao Yan*,§

Department of Biochemistry and Molecular Biology, Michigan State University, East Lansing, Michigan 48824, and Macromolecular Crystallography Laboratory, National Cancer Institute, P.O. Box B, Frederick, Maryland 21702

Received November 17, 2003

ABSTRACT: 6-Hydroxymethyl-7,8-dihydropterin pyrophosphokinase (HPPK) catalyzes the transfer of pyrophosphoryl group from ATP to 6-hydroxymethyl-7,8-dihydropterin (HP) following an ordered bi−bi mechanism with ATP as the first substrate. The rate-limiting step of the reaction is product release, and the complete active center is assembled and sealed only upon the binding of both ATP and HP. The assembly of the active center involves large conformational changes in three catalytic loops, among which loop 3 undergoes the most dramatic and unusual changes. To investigate the roles of loop 3 in catalysis, we have made a deletion mutant, which has been investigated by biochemical and X-ray crystallographic analysis. The biochemical data showed that the deletion mutation does not have significant effects on the dissociation constants or the rate constants for the binding of the first substrate MgATP or its analogues. The dissociation constant of HP for the mutant increases by a factor of ∼100, which is due to a large increase in the dissociation rate constant. The deletion mutation causes a shift of the rate-limiting step in the reaction and a decrease in the rate constant for the chemical step by a factor of $\sim 1.1 \times 10^5$. The crystal structures revealed that the deletion mutation does not affect protein folding, but the catalytic center of the mutant is not fully assembled even upon the formation of the ternary complex and is not properly sealed. The results together suggest that loop 3 is dispensable for the folding of the protein and the binding of the first substrate MgATP, but is required for the assembling and sealing of the active center. The loop plays an important role in the stabilization of the ternary complex and is critical for catalysis.

6-Hydroxymethyl-7,8-dihydropterin pyrophosphokinase (HPPK)[1] catalyzes the transfer of pyrophosphate from ATP to 6-hydroxymethyl-7,8-dihydropterin (HP; Figure 1a), leading to the biosynthesis of folate cofactors (*1*). Folate cofactors are essential for life (*2*). Mammals have an active transport system for deriving folates from their diet. In contrast, most microorganisms must synthesize folates de novo because they lack the active transport system. Therefore, like other enzymes in the folate pathway, HPPK is an attractive target for developing antimicrobial agents.

Phosphoryl transfer catalyzed by kinases takes place at the γ-phosphorus of nucleoside triphosphate (NTP), whereas pyrophosphoryl transfer catalyzed by pyrophosphokinases takes place at the β-phosphorus (*3*, *4*). The structure and mechanism of kinases have been intensely studied for decades, but the structural and mechanistic studies of pyrophosphokinases have just begun in earnest recently (*5*−*12*). As a small (∼18 kDa), stable, monomeric protein, HPPK is also an excellent model system for studying the catalytic mechanisms of enzymatic pyrophosphoryl transfer.

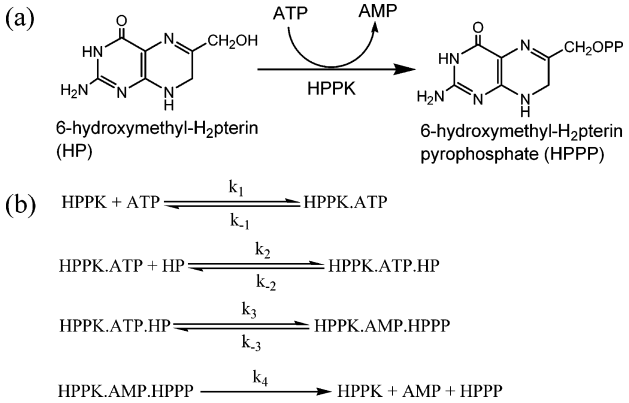

FIGURE 1: Pyrophosphoryl transfer reaction catalyzed by HPPK (a) and kinetic mechanism (b). Mg^{2+} is required for the reaction, but for simplicity, Mg^{2+} is not shown in the kinetic scheme.

Comparative analysis of the crystal structures of ligand-free HPPK and its ternary complex with HP and an ATP analogue has revealed that the complete active center of HPPK is assembled only after both substrates bind to the enzyme (*8*). The assembly of the active center involves large conformational changes, particularly in the catalytic loops 1−3, among which loop 3 undergoes dramatic and unusual

† This work was supported in part by NIH Grant GM58221 (H.Y.).

* To whom correspondence should be addressed. Phone: (517) 353-8786 (H.Y.); (301) 846-5035 (X.J.). Fax: (517) 353-9334 (H.Y.); (301) 846-6073 (X.J.). E-mail: yanh@msu.edu (H.Y.); jix@ncifcrf.gov (X.J.).

‡ National Cancer Institute.

§ Michigan State University.

|| Current address: Division of Nephrology, S-3322, MCN, Vanderbilt University School of Medicine, Nashville, TN 37232.

[1] Abbreviations: AMPCPP, α,β-methyleneadenosine triphosphate; Ant-ATP, 3′(2′)-*O*-anthraniloyladenosine 5′-triphosphate; GST, glutathione S-transferase; HP, 6-hydroxymethyl-7,8-dihydropterin; HPPK, 6-hydroxymethyl-7,8-dihydropterin pyrophosphokinase; NTP, nucleoside triphosphate; HPO, 6-hydroxymethylpterin; rmsd, root-mean-square deviation.

10.1021/bi036053l CCC: $27.50 © 2004 American Chemical Society
Published on Web 01/17/2004

changes (*13*). Before moving in and closing the active center, loop 3 moves in the opposite direction upon the binding of nucleotide; residues in the loop move as much as ~17 Å, and the hand-shaped molecule appears to be opening up. This unusual conformational change appears to be necessary to bring catalytic residues R82 and R92 into the active center (*13*). At 0.89 Å resolution, two distinct conformations have been observed for R82 and R92 in the crystal structure of HPPK in complex with two HP variants, two Mg^{2+} ions, and an ATP analogue (*14*). Structural information suggests that R92 first binds to the α-phosphate group of ATP and then shifts to interact with *β*-phosphate as R82 moves in and binds to α-phosphate when the pyrophosphoryl transfer is about to occur. The roles of R82 and R92 in HPPK catalysis are further elucidated by biochemical studies (*15*) and five more crystal structures of two mutant proteins, R82A and R92A, with and without bound ligands (*14*).

In this paper, we describe the site-directed mutagenesis, biochemical, and X-ray crystallographic studies of loop 3. We show that loop 3 is dispensable for the folding of the protein and the binding of the first substrate MgATP but is required for the assembling and sealing of the active center. The loop plays an important role in the stabilization of the ternary complex and is critical for catalysis.

EXPERIMENTAL PROCEDURES

Materials. ATP and α,*β*-methyleneadenosine triphosphate (AMPCPP, an ATP analogue and dead-end inhibitor for HPPK-catalyzed pyrophosphoryl transfer) were purchased from Sigma. 6-Hydroxymethylpterin (HPO) was synthesized according to Thijssen (*16*) and had the same UV absorption and NMR spectra as that purchased from Sigma. HP was prepared from HPO by reduction with sodium dithionite (*17*) or purchased from Schircks Laboratories.

Mutant Construction and Protein Purification. The deletion mutant V83GΔ84−89 was made by a PCR-based method using high-fidelity *pfu* DNA polymerase according to a protocol developed by Stratagene. The forward and reverse primers for making the mutant were 5′-GAATTGCAGCAAGGTCGCGGCGGACCACGCACGCTGG-3′ and 5′-CCAGCGTGCGTGGTCCGCCGCGACCTTGCTGCAATTC-3′. The mutant was selected by DNA sequencing. To ensure that there were no unintended mutations in the mutant, the entire sequence of the mutated gene was determined. The mutant protein was purified as previously described for the wild-type enzyme (*18*).

Construction and Purification of HPPK−GST Fusion Proteins. The gene for the mutant was subcloned into the *Nde*I and *Bam*HI sites of a homemade expression vector (pET14b-3T) derived from the Novagen vector pET14b. The mutant protein was fused to glutathione S-transferase (GST) with a link that included a thrombin cleavage site. The fusion protein was purified with a glutathione agarose column and digested with thrombin. The thrombin-digested proteins were run through a Sephadex G-75 column. The HPPK fractions were located by SDS−PAGE and concentrated by an Amicon cell with anYM10 membrane disk.

Thermodynamic Analysis. The K_d values for various ligands were measured by fluorometric titration at 24 °C on a Spex FluoroMax-2 fluorometer as previously described (*9*, *18*). The titration experiments were performed in a single cuvette so that both protein and ligand concentrations varied with the addition of each aliquot of a stock solution. The independent variable in the experiment was the volume of the added stock solution. To determine the dissociation constant of 3′(2′)-*O*-anthraniloyladenosine 5′-triphosphate (Ant-ATP, a fluorescent analogue of ATP), 3 *μ*M V83GΔ84−89 was titrated with Ant-ATP in 100 mM Tris−HCl, 10 mM $MgCl_2$, pH 8.3. The excitation wavelength and slit were 370 and 1 nm, respectively. The emission wavelength and slit were 425 and 5 nm, respectively. A set of control data was obtained in the absence of the protein, which was then subtracted from the corresponding data set obtained in the presence of protein after correction of inner filter effects. The dissociation constant for Ant-ATP was obtained by a nonlinear least-squares fit of the subtracted data (*18*).

The dissociation constants for nonfluorescent nucleotides were measured by a competitive binding assay as previously described (*9*). Briefly, a solution containing 10 *μ*M V83GΔ84−89 and 10 *μ*M Ant-ATP in 100 mM Tris−HCl, 10 mM $MgCl_2$, pH 8.3, was titrated with ATP or AMPCPP. The excitation wavelength and slit were 337 and 1 nm, respectively. The emission wavelength and slit were 425 and 5 nm, respectively. The fluorometric data were fitted by a nonlinear least-squares method (*9*).

To determine the K_d value for HP, a solution containing 0.55 *μ*M HP and 200 *μ*M AMPCPP in 50 mM Bicine, 10 mM $MgCl_2$, 25 mM DTT, pH 8.3, was titrated with V83GΔ84−89 (*9*). The excitation wavelength and slit were 330 and 5 nm, respectively. The emission wavelength and slit were 430 and 10 nm, respectively. A control titration experiment was performed in the absence of HP, the data set of which was subtracted from the corresponding data set obtained in the presence of HP. The data were then analyzed by a nonlinear least-squares method (*9*).

Stopped-Flow Analysis. Stopped-flow experiments were performed in an Applied Photophysics SX.18MV-R stopped-flow spectrofluorometer as previously described (*9*). To measure the binding of MgAMPCPP, a solution containing V83GΔ84−89 was mixed rapidly with a solution containing AMPCPP, $MgCl_2$, and HP at 25 °C. Fluorescence traces were obtained with an excitation wavelength of 340 nm and a filter with a cutoff of 395 nm for emission. The concentrations of V83GΔ84−89, HP, and $MgCl_2$ were fixed at 1 *μ*M, 20 *μ*M, and 10 mM, respectively. AMPCPP was varied from 5 to 30 *μ*M.

To measure the binding of HP, a solution containing V83GΔ84−89, AMPCPP, and $MgCl_2$ was mixed rapidly with a solution containing HP at 25 °C. Fluorescence traces were obtained with an excitation wavelength of 330 nm and a filter with a cutoff of 395 nm for emission. The concentrations of HP, AMPCPP, and $MgCl_2$ were fixed at 1 *μ*M, 30 *μ*M, and 10 mM, respectively. V83GΔ84−89 was varied from 2 to 16 *μ*M. All concentrations were those right after the rapid mixing. The rate constants were evaluated by numerical analysis of the stopped-flow data using the program DYNAFIT (*19*).

Quench-Flow Analysis. Quench-flow experiments were carried out with a KinTek RQF-3 rapid quench-flow instrument as previously described (*9*). All reaction components were dissolved in 100 mM Tris−HCl buffer, pH 8.3. A trace amount of [α-^{32}P]ATP was used to follow the reactions. The reactions were initiated with Mg^{2+} at 30 °C and quenched

Table 1: Ligand-Binding Properties of Wild-Type HPPK and the Deletion Mutant

	WT	V83GΔ84−89		WT	V83GΔ84−89
$K_{d(MgAntATP)}$ (μM)	1.6 ± 0.05	4.0 ± 0.1	$K_{d(MgAMPCPP)}$ (μM)	0.077 ± 0.006[b]	0.32 ± 0.01
$K_{d(MgATP)}$ (μM)	2.6 ± 0.06[a]	7.1 ± 0.07	$K_{d(HP)}$ (μM)	0.17 ± 0.01[b]	18 ± 1

[a] From Shi et al. (*18*). [b] From Li et al. (*9*).

Table 2: Kinetic Parameters of Wild-Type HPPK and the Deletion Mutant

	WT[a]	WT* [c]	V83GΔ84−89
k_1 (μM^{-1} s^{-1})	0.27 ± 0.001		
	0.3 ± 0.02[b]		0.27 ± 0.005[b]
k_{-1} (s^{-1})	0.95 ± 0.001		
	0.023 ± 0.002[b]		0.068 ± 0.002[b]
k_2 (μM^{-1} s^{-1})	11 ± 0.03		12 ± 0.03
k_{-2} (s^{-1})	2.0 ± 0.04		180 ± 3
k_3 (s^{-1})	16 ± 1	25 ± 2	(2.3 ± 0.09) × 10^{-4} [d]
k_{-3} (s^{-1})	20 ± 1	27 ± 4	
k_4 (s^{-1})	1.8 ± 0.1	1.3 ± 0.1	
k_{cat} (s^{-1})	0.76	0.61	

[a] From Li et al. (*9*). [b] Measured for MgAMPCPP (this work). [c] WT*, wild-type HPPK with four extra residues, Gly-Ser-His-Met, at the N-terminus. [d] Measured for V83GΔ84−89* with four extra residues, Gly-Ser-His-Met, at the N-terminus.

with 500 mM EDTA. The substrates and products were separated by thin-layer chromatography on a plastic sheet coated with PEI-cellulose developed with 0.25 M NaH_2PO_4. The radioactivity was quantified by a Molecular Dynamics Storm 820 Phosphor-Imager. The reaction mixture contained 10 μM V83GΔ84−89, 100 μM ATP, 110 μM HP, 25 mM DTT, 0.5 mM EDTA, and 10 mM $MgCl_2$ in 100 mM Tris−HCl buffer, pH 8.3. The pre-steady-state data were first analyzed by nonlinear least-squares fit of the data to eq 1. The amplitudes and rate constants were then used to set the initial values for fitting the data to the complete mechanism by numerical analysis using the program DYNAFIT (*19*).

$$[\mathrm{AMP}]/[\mathrm{HPPK}] = A(1 - e^{-\lambda t}) + k_{cat}t \qquad (1)$$

Crystallographic Analysis. V83GΔ84−89 and its complex with MgAMPCPP and HP were crystallized at room temperature (19 ± 1 °C) using the hanging-drop vapor-diffusion technique. The drops were formed by mixing equal volumes of protein solution and reservoir solution (Table 1). Crystals of apo-V83GΔ84−89 appeared after 2−3 days, and after about 3 weeks they grew to the size suitable for data collection (Table 3). Ternary complex V83GΔ84−89·MgAMPCPP·HP crystallized in two forms, monoclinic and orthorhombic, under exactly the same conditions (Table 3). However, a longer time was needed for orthorhombic crystals. Monoclinic crystals appeared overnight and grew, in a few days, to the size suitable for the X-ray diffraction experiment. Orthorhombic crystals were noticed after about 2 months of incubation.

X-ray diffraction data were collected from the single crystals at cryogenic temperature (100 K), with an ADSC Quantum-4 CCD detector mounted at the synchrotron beamline X9B at the National Synchrotron Light Source, Brookhaven National Laboratory. The details of the data collection are summarized in Table 4. The apo-V83GΔ84−89 crystal belongs to space group $P2_12_12_1$ with cell parameters a = 41.266 Å, b = 41.685 Å, and c = 77.896 Å. The orthorhombic V83GΔ84−89·MgAMPCPP·HP crystal belongs to $P2_12_12$ with a = 51.609 Å, b = 63.156 Å, and c = 36.201 Å, and its monoclinic form belongs to $P2_1$ with a = 52.797 Å, b = 68.752 Å, c = 36.491 Å, and β = 90.50°. Data processing was carried out with the HKL2000 program suite (*20*). The crystal structures were solved using the molecular replacement program AmoRe (*21*). The search model for apo-V83GΔ84−89 was the 1.5 Å structure of apo-HPPK (PDB code 1hka, *5*), and that for the ternary complex was the 1.25 Å structure of HPPK·MgAMPCPP·HP (PDB code 1eqo, *8*). Solvent molecules and residues 83−89 were removed from both search models. The initial refinement was carried out with the simulated annealing methods using CNS (*22*), followed by the least-squares refinement using SHELXL-97 (*23*). All graphics work, including model adjustments, building, and rebuilding, was carried out using O (*24*).

All three structures were refined with anisotropic temperature factors for non-hydrogen atoms, excluding those in regions with highly increased mobility. Hydrogen atoms of protein and cofactors were built geometrically at their idealized positions and assigned with isotropic thermal parameters equal to 1.2 times the equivalent isotropic thermal parameters of their parent atoms. Positional parameters of ligands and ions have been refined with geometric restrictions for bond lengths, valence angles, and planarity. The geometry of finalized structures was assessed using PROCHECK (*25*). The details of refinement and statistics of the final structures are summarized in Table 4. Schematic representations of apo-V83GΔ84−89 and V83GΔ84−89·MgAMPCPP·HP are shown in Figure 2.

RESULTS

Mutant Design. Loop 3, which connects α-helix 2 (α2) and β-strand 4 (β4) and is delimited by strictly conserved R82 and R92 (Figure 2), undergoes dramatic conformational changes in the catalytic cycle as revealed by our recent crystal and NMR solution structures (*5*, *8*, *13*). To investigate the role of the loop in HPPK catalysis, we made a deletion mutant by removing most of loop 3 but keeping R82 and R92, knowing that R82 and R92 play important roles in catalysis (*14*, *15*). Molecular modeling suggested that a three-residue link should be sufficient to connect R82 and R92. Residues 90 and 91 are glycine and proline, respectively, and are suitable as link residues. Therefore, we replaced V83 with glycine and deleted residues 84−89 to create the deletion mutant V83GΔ84−89. G83, G90, and P91 served as the three-residue link connecting α2 and β4 (Figure 2).

Deletion of Loop 3 Has a Significant Impact on the Binding of HP but Not ATP. The HPPK-catalyzed reaction follows an ordered bi−bi mechanism (*26*). We have previously established a thermodynamic and kinetic framework for the reaction by a combination of thermodynamic and transient kinetic analyses (Figure 1) (*9*). The same approach was used for the characterization of V83GΔ84−89. The K_d value of MgAnt-ATP was determined first, and those of other

Table 3: Summary of Crystallization of Apo-V83GΔ84−89 and Two Forms of V83GΔ84−89·MgAMPCPP·HP

	apo-V83GΔ84−89	V83GΔ84−89·MgAMPCPP·HP	
Protein Solution			
protein concn (mg/mL)	9	9	
HP concn (mM)		15	
$MgCl_2$ concn (mM)		50	
buffer	0.1 M Tris−HCl, pH 8	0.1 M Tris−HCl, pH 8	
Reservoir Solution			
PEG 4000 concn (%, w/v)	30	30	
sodium acetate concn (M)	0.2		
ammonium acetate concn (M)		0.2	
$MgCl_2$ concn (mM)	50		
glycerol concn (%, v/v)	5	1	
buffer	0.1 M Tris−HCl, pH 8.5	0.1 M sodium acetate, pH 4.6	
Crystal			
form		orthorhombic	monoclinic
shape	block	plate	plate
dimensions (mm^3)	0.05 × 0.10 × 0.35	0.07 × 0.30 × 0.30	0.01 × 0.20 × 0.30

Table 4: Summary of Structure Solution and Refinement of Apo-V83GΔ84−89 and Two Forms of V83GΔ84−89·MgAMPCPP·HP

	apo-V83GΔ84−89	V83GΔ84−89·MgAMPCPP·HP	
X-ray Diffraction Data			
space group	$P2_12_12_1$	$P2_12_12$	$P2_1$
resolution (Å)	1.33	1.48	1.40
no. of Measured reflns	326883	152250	133032
no. of unique reflns	30708	20535	49585
completeness (%), overall/last shell[a]	97.1/95.4	99.8/99.9	93.9/89.0
R_{merge},[b] overall/last shell	0.083/0.481	0.132/0.599	0.061/0.541
$I/\sigma(I)$, overall/last shell	26.8/5.3	14.6/1.9	14.0/1.9
Molecular Replacement			
search model (PDB code)	1hka	1eqo	1eqo
correlation coeff	0.63	0.65	0.59
R-factor	0.38	0.38	0.42
Refinement and Statistics			
no. of reflns in refinement	29123	19335	45829
no. of reflns for R_{free}	1541	1015	2421
no. of residues/non-H atoms	152/1285	146/1169	296/2933
no. of heterogeneous atoms	6	48	95
no. water oxygen atoms	228	130	481
final R_{free}	0.167	0.197	0.197
final *R*-factor	0.134	0.172	0.149
rms dev (Å)			
bond lengths	0.013	0.009	0.010
bond angles	0.033	0.029	0.030
estimated coordinate error (Å)	0.107	0.154	0.127
overall B_{iso} ($Å^2$, excluding solvent)	19.2	28.3	19.2
Wilson *B*-factor (Å)	16.6	24.2	18.7
Ramachandran statistics (%)			
most favored φ/ψ values	94.6	96.8	96.0
disallowed φ/ψ values	0	0	0

[a] 1.38−1.33 Å. [b] $R_{merge} = \sum|(I - \langle I\rangle)|/\sum(I)$, where *I* is the observed intensity.

nucleotides were then determined by a competitive binding assay monitoring the fluorescent changes caused by the displacement of MgAnt-ATP (Figure 3a). The dissociation constants of HP were measured in the presence of MgAMPCPP (Figure 3b). The K_d values of MgAMPCPP allowed us to design the experiment so that the protein was saturated with the nucleotide. The results of the thermodynamic analysis are summarized in Table 1. The K_d values of ATP or ATP analogues for V83GΔ84−89 were similar to that of the wild type. The largest difference was a 3-fold increase in the K_d value for MgAMPCPP. However, the K_d value for HP was ~100-fold higher than that for the wild type.

We then determined the rate constants for the binding of the substrates by stopped-flow analysis. The binding of MgATP to the wild-type HPPK could be measured by monitoring the small but significant change in the protein fluorescence. The fluorescence change was attributed to W89. Because W89 was removed in the deletion mutant, there was little change in the protein fluorescence upon MgATP binding. However, there was a dramatic change in the fluorescence of HP upon its binding to V83GΔ84−89, and therefore, the binding of HP could be measured with stopped-flow fluorometry. To avoid the chemical reaction, the kinetics of HP binding was measured in the presence of MgAMPCPP instead of MgATP. The protein was preincubated with an excess of MgAMPCPP in one syringe and then mixed with HP because the binding of MgAMPCPP and HP follows an ordered process, with the binding of MgAMPCPP first. When HPPK was incubated first with MgAMPCPP and then mixed with HP, the fluorescent change reflected the kinetics of HP binding. On the other hand, when HPPK was mixed with both MgAMPCPP and HP at the same time, the fluorescent

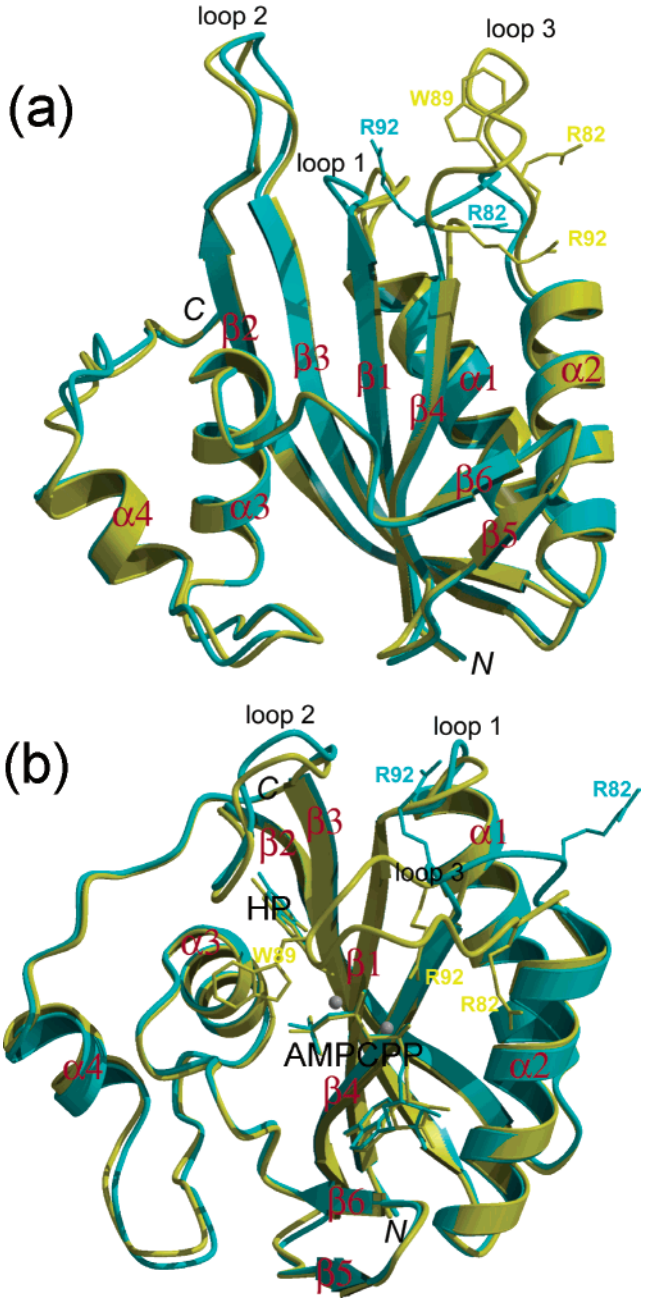

FIGURE 2: Schematic representation of the crystal structures of V83GΔ84−89. (a) Ligand-free V83GΔ84−89 (in cyan) is superimposed with apo-HPPK (*5*). (b) Mol B of the monoclinic form V83GΔ84−89·MgAMPCPP·HP (in cyan) is superimposed with HPPK·AMPCPP·HP (*8*). Secondary structure elements are shown as spirals for α-helices, arrows for *β*-strands, and pipes for loops. Ligands and side chains of R82, W89, and R92 are shown as stick models with the color scheme of the respective protein molecule to which they are associated. This illustration was made with Bobscript (*28*) and Raster3D (*29*).

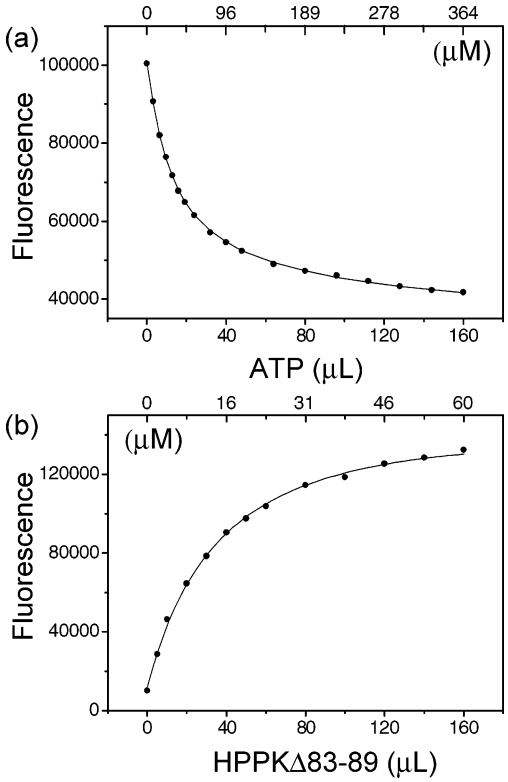

FIGURE 3: Thermodynamic analysis of the binding of MgATP (a) and HP (b) to V83GΔ84−89. (a) A solution containing 10 μM V83GΔ84−89 and 10 μM Ant-ATP in 100 mM Tris−HCl, 10 mM $MgCl_2$, pH 8.3, was titrated with ATP at 24 °C. The concentration of the ATP stock solution was 4.9 mM. The top axis indicates the concentrations of ATP during the titration. (b) A solution containing 0.55 μM HP and 100 μM AMPCPP in 100 mM Tris−HCl, 10 mM $MgCl_2$, 25 mM DTT, pH 8.3, was titrated with V83GΔ84−89 at 24 °C. The concentration of the V83GΔ84−89 stock solution was 810 μM. The top axis indicates the concentrations of the mutant protein during the titration. The solid lines in both panels were obtained by nonlinear least-squares analysis.

change reflected mainly the kinetics of MgAMPCPP binding because HP binding was much faster. Since we had already measured the rate constants for HP binding, we were able to measure, precisely, the rate constants for the binding of MgAMPCPP, in the presence of excess HP, by monitoring the fluorescence change of HP. The stopped-flow analysis for the binding of MgAMPCPP and HP is shown in Figure 4. The rate constants are listed in Table 2. Both association and dissociation rate constants of MgAMPCPP for V83GΔ84−89 were very similar to those for the wild-type HPPK. Although the association rate constant of HP for V83GΔ84−89 was similar to that of the wild type, the rate constant for the dissociation of HP increased by a factor of 90. The dissociation constants calculated from the rate constants (transient kinetic analysis) were consistent with those measured by the fluorometric titrations (thermodynamic analysis).

Deletion of Loop 3 Causes a Shift of the Rate-Limiting Step. The catalytic properties of V83GΔ84−89 were measured by quench-flow analysis (Figure 5a). Because the *E. coli* strain BL21(DE3) used to produce the mutant proteins contained a wild-type gene for HPPK in its chromosome and the same procedure was used to purify the wild-type and mutant proteins, the preparation of the mutant contained a minute amount of the wild type, estimated to be <0.1% on the basis of the expression levels of the genes. The minute contamination of the wild type did not have any significant effects on the measurements of the ligand-binding properties of the mutant, but it was sufficient to affect the kinetics, especially when the mutant had an extremely low catalytic activity as we observed earlier (*15*).

To eliminate the contamination of the wild-type HPPK, a plasmid construct was made by fusing the mutant gene to the gene encoding GST. The GST-fusion protein of V83GΔ84−89 was purified by affinity chromatography with

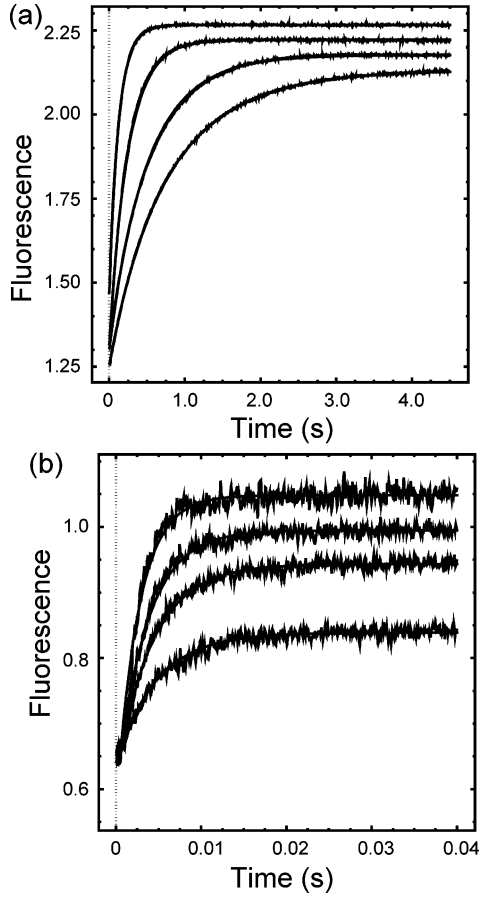

FIGURE 4: Stopped-flow analysis of the binding of MgAMPCPP (a) and HP (b) to V83GD84−89. (a) The concentrations of V83GΔ84−89, HP, and $MgCl_2$ were fixed at 1 μM, 20 μM, and 10 mM, respectively. The concentrations of AMPCPP were 5, 7.5, 15, and 30 μM for traces from bottom to top, respectively. (b) The concentrations of HP, AMPCPP, and $MgCl_2$ were fixed at 1 μM, 30 μM, and 10 mM, respectively. The concentrations of V83GΔ84−89 were 2, 4, 8, and 16 μM for traces from bottom to top, respectively. All concentrations refer to the concentrations right after the rapid mixing. The solid lines were obtained by global fitting using the program DYNAFIT (*19*).

a glutathione agarose column, thus eliminating the wild-type HPPK produced by the chromosomal gene. The GST moiety was removed by thrombin cleavage, leaving the V83GΔ84−89 protein with four extra residues, Gly-Ser-His-Met, at the N-terminus (V83GΔ84−89*). Previously, we demonstrated that the kinetics of the thus prepared wild-type HPPK (WT*; Figure 5b) and that of the native HPPK were very similar (*9*). The time course consists of two phases, a burst phase and a steady-state phase, as described by eq 1. The burst phase is characterized by two constants, amplitude A and rate constant λ. The steady-state phase is characterized by rate constant k_{cat}. The three constants are related to the rate constants in Figure 1 according to the following equations (*27*):

$$A = \frac{k_3(k_3 + k_{-3})}{(k_3 + k_{-3} + k_4)^2} \quad (2)$$

$$\lambda = k_3 + k_{-3} + k_4 \quad (3)$$

$$k_{cat} = \frac{k_3 k_4}{k_3 + k_{-3} + k_4} \quad (4)$$

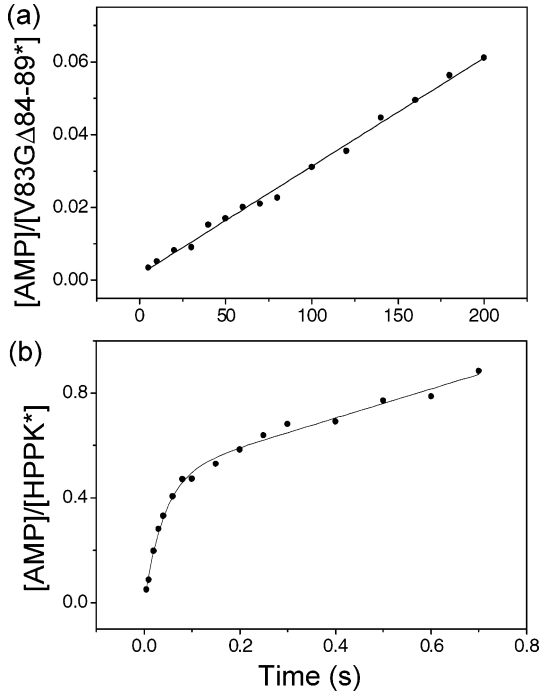

FIGURE 5: Quench-flow analysis of V83GΔ84−89* (a) and HPPK* (b). The asterisks indicate four extra residues, Gly-Ser-His-Met, at the N-termini of the enzymes. The reaction mixture contained 10 μM enzyme (V83GΔ84−89* or HPPK*), 100 μM ATP, 110 μM HP, 25 mM DTT, 0.5 mM EDTA, and 10 mM $MgCl_2$ in 100 mM Tris−HCl buffer, pH 8.3. The reaction was initiated by mixing with $MgCl_2$ at 30 °C and quenched by mixing with EDTA. The solid lines were obtained by nonlinear least-squares fit to eq 4 as described in the Experimental Procedures.

The amplitude and rate constants for the two phases of the reaction were evaluated by nonlinear least-squares fit to eq 4. The individual rate constants were then estimated according to eqs 2−4 and used to set the initial values for the numerical analysis using the program DYNAFIT (*19*). The values for the individual rate constants of the wild-type HPPK and the mutants are listed in Table 2. The k_{cat} values were calculated according to eq 4 and are also listed in Table 2.

No burst kinetics was observed for the deletion mutant V83GΔ84−89* (Figure 5a), indicating that the chemical step is rate limiting. The rate constant obtained by least-squares linear regression was 2.3×10^{-4} s^{-1}. Because the chemical step was rate limiting, the rate constant for the deletion mutant was for the chemical step instead of product release as for the wild-type HPPK. Therefore, the deletion mutation caused a decrease in the rate constant for the chemical step by a factor of $\sim 1.1 \times 10^5$ (25 s^{-1} for WT* vs 2.3×10^{-4} s^{-1} for V83GΔ84−89*).

Deletion of Loop 3 Does Not Affect Protein Folding. To assess the structural effects of the deletion mutation, we determined three crystal structures, including apo-V83GΔ84−89 (space group $P2_12_12_1$) and two forms of V83GΔ84−89·MgAMPCPP·HP ($P2_12_12$ and $P2_1$, respectively) at high resolutions (Table 4). In the asymmetric unit, apo-V83GΔ84−89 has one V83GΔ84−89 molecule, and the orthorhombic V83GΔ84−89·MgAMPCPP·HP has one ternary complex, but the monoclinic V83GΔ84−89·MgAMPCPP·HP has two complexes, Mol A and Mol B. Therefore, one copy of apo-V83GΔ84−89 and three copies of V83GΔ84−89·

MgAMPCPP·HP have been determined independently. The entire polypeptide chain of V83GΔ84−89 in the apo structure is well defined, which is shown in Figure 2a. However, among the three copies of V83GΔ84−89·MgAMPCPP·HP, only Mol B of the monoclinic crystal has a continuous polypeptide chain (Figure 2b). In Mol A of the monoclinic complex, residues 45−50, 83, 90, and 91 do not have electron density. In the orthorhombic complex, residues 45−50 do not have electron density. The missing residues are assumed disordered. All protein-bound ligand and solvent molecules have well-defined electron density. A total of 16, 2, 2, and 6 side chains assume two conformations in apo $P2_12_12_1$, ternary $P2_12_12$, ternary $P2_1$ Mol A, and ternary $P2_1$ Mol B, respectively. Apo-V83GΔ84−89 has the largest number of side chains with dual conformations, reflecting a more dynamic nature of the ligand-free enzyme.

The deletion mutation does not affect the folding of the enzyme. The Cα trace of apo-V83GΔ84−89 superimposes well with apo-HPPK (*5*) (Figure 2a). The root-mean-square deviation (rmsd) between all Cα atoms of the mutant and the wild type is 0.91 Å. In addition to residues 78−83 and 90−93 located in the immediate vicinity of the deletion mutation, residues 10−13 (loop 1), 44−54 (loop 2), and 150−153 (C-terminus) have higher deviations (Figure 2a). Excluding these residues, the rmsd value (0.91 Å) decreases to 0.49 Å.

The ternary complex of V83GΔ84−89 revealed by the crystal structure of V83GΔ84−89·MgAMPCPP·HP is the same as HPPK·MgAMPCPP·HP (*8*). The Cα trace of three copies of V83GΔ84−89 and that of wild-type HPPK superimpose very well. So do the bound ligands in the four structures. The Cα alignment between Mol B of monoclinic V83GΔ84−89·MgAMPCPP·HP and HPPK·MgAMPCPP·HP (*8*) is shown in Figure 2b. Significant deviations are found in the vicinity of the mutation, loop 1, and loop 2 regions. Excluding these regions, the rmsd between the Cα atoms of the mutant and the wild type is 0.41, 0.59, and 0.51 Å for ternary $P2_12_12$, ternary $P2_1$ Mol A, and ternary $P2_1$ Mol B, respectively.

The protein−ligand interactions observed in HPPK·MgAMPCPP·HP (*8*) are largely retained in all three copies of V83GΔ84−89·MgAMPCPP·HP. The Mg^{2+} coordinations are identical in the mutant and the wild type. Of the six hydrogen bonds between the enzyme and HP, all are identical except for two hydrogen bonds involving L45. These two hydrogen bonds are invisible in ternary $P2_12_12_1$ and $P2_1$ Mol A because residues 45−50 are missing. In ternary $P2_1$ Mol B, loop 2 is defined and the hydrogen bond between atom N1 of HP and atom NH of L45 exists but the one between atom N8 of HP and atom O of L45 is lost due to the flip of the peptide bond between residues 45 and 46. Among the hydrogen bonds between the adenosine moiety of AMPCPP and protein, only the one between the guanidinium group of R84 and the 3′-hydroxyl group of the ribose is lost because of the deletion of residues 84−89. Of the hydrogen bonds between the triphosphate of AMPCPP and protein, all but those involving W89, R82, and R92 are retained. The loss of the hydrogen bond with W89 is due to the deletion mutation, whereas the loss of hydrogen bonds involving R82 and R92 is because the two side chains can no longer move into the active center of the enzyme.

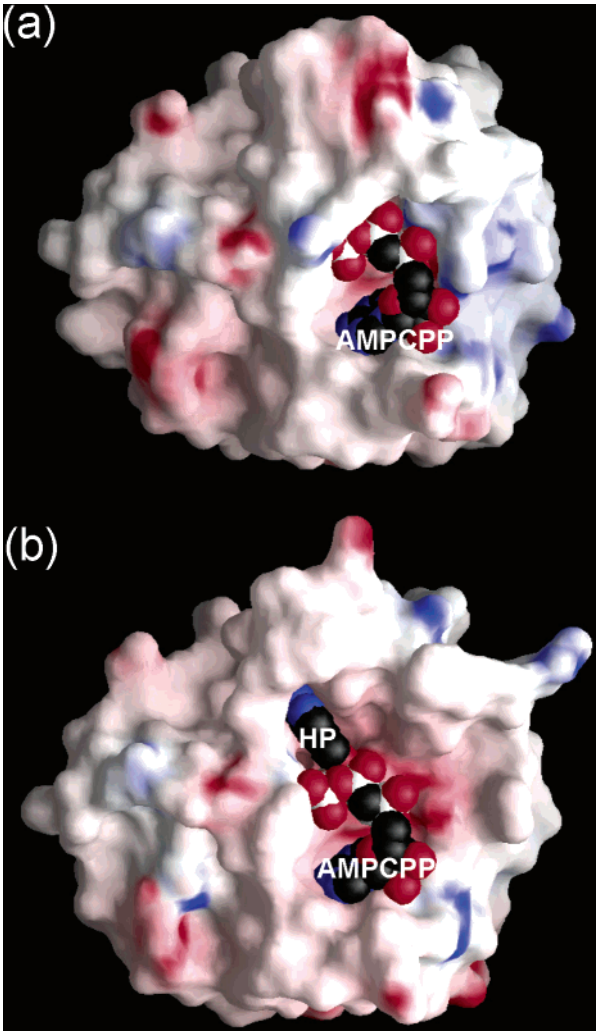

FIGURE 6: Space-filling models of the ternary complexes. (a) The active center is properly sealed for catalysis in HPPK·AMPCPP·HP. (b) V83GΔ84−89·AMPCPP·HP has an exposed catalytic center. The protein is shown as a surface representation with negative and positive potentials indicated by red and blue colors, respectively. The bound ligands are shown as van der Waals spheres in an atomic color scheme (black, carbon; blue, nitrogen; red, oxygen; white, phosphorus). This figure was created using Grasp (*30*).

Deletion of Loop 3 Excludes R82 and R92 from the Catalytic Center Assembly. Arginine residues 82 and 92, strictly conserved in 35 HPPK sequences, play important roles in the catalytic cycle of the enzyme (*14*, *15*). In apo-HPPK (*5*), both R82 and R92 point out from the active center (Figure 2a), whereas in HPPK·MgAMPCPP·HP (*8*), they move into the active center and participate in the formation of the catalytic center assembly (Figure 2b). This movement is facilitated by the dramatic conformational change of loop 3, which occurs during the formation of the ternary complex (*13*). In V83GΔ84−89, loop 3 of which is significantly smaller and therefore stiffer, the two guanidinium groups can no longer move into the active center (Figure 2). Consequently, they are excluded from the catalytic center assembly, which must have a significant impact on catalysis.

V83GΔ84−89 Cannot Seal the Active Center Properly. Our crystal structure of HPPK·MgAMPCPP·HP (*8*) shows that the enzyme properly seals the active center where the reaction occurs (Figure 6a). Without loop 3, however,

V83GΔ84−89 can no longer seal the active center properly (Figure 6b), which must have a dramatic impact on catalysis.

DISCUSSION

The kinetics of the HPPK-catalyzed reaction follows an ordered bi−bi mechanism, with the binding of MgATP first. In apo-HPPK (*5*), the side chains of several conserved residues, including R82 and R92, point away from the active center (Figure 2a). The catalytic center is assembled only after the binding of both substrates and the moving in of the functional groups of R82 and R92 (Figure 2b), which involves the movements of three catalytic loops and the formation of a network of six hydrogen bonds anchored by N10 that is located at the beginning of loop 1 (*8*). Among the three loops, loop 3 undergoes unusual and dramatic conformational changes that are coupled to the conformational changes of loops 1 and 2, which stabilizes the ternary complex and seals the active center for the reaction to occur (*8*, *13*). In this study, we have shown that loop 3 is dispensable in the binding of MgATP but plays a significant role in HP binding. The results suggest that the energy of the hydrogen bond formation may be used to pay for the coupled conformational changes of loops 1−3 rather than the increase of the affinity between the nucleotide and the enzyme. The significant decrease of the affinity for HP is due to the increase in the dissociation rate constant. The rapid dissociation of HP is likely due to the increased flexibility of loop 2 in the deletion mutant, which is caused by the deletion of loop 3, resulting in the decoupling of the two loops.

The deletion of loop 3 shifts the rate-limiting step in the reaction. The wild-type HPPK shows a classical burst kinetic behavior (Figure 5b); the rate-limiting step is product release rather than chemical transformation (*9*). No burst kinetics is observed for V83GΔ84−89 (Figure 5a), indicating that the chemical step is rate limiting and that the rate constant for the chemical step is very close to k_{cat}. The deletion of loop 3 causes a decrease in the rate constant for the chemical step by a factor of $\sim 1.1 \times 10^5$, corresponding to a 6.9 kcal/mol change of free energy in the transition state, indicating that loop 3 is critical for HPPK catalysis. X-ray crystallographic analysis of the mutant indicates that loop 3 is required for assembling and sealing the catalytic center of the ternary complex. The dramatic effect of the loop 3 deletion on HPPK catalysis is apparently due to the inability of the mutant to fully assemble (Figure 2) and properly seal the active center (Figure 6).

As described earlier, loop 3 is delimited by R82 and R92 (Figure 2). Therefore, it is of great interest to compare the properties of V83GΔ84−89 with point mutants R82A and R92A (*14*, *15*). While the K_d values and rate constants of all three mutants and the wild type for the binding of MgATP (the first substrate) are similar, their K_d values and rate constants for the binding of HP (the second substrate) behave differently: For R82A, the K_d value and rate constants are similar to those of the wild type. For R92A, the K_d value is similar to that, but its rate constants are significantly smaller than those, of the wild type. For V83GΔ84−89, the K_d value is substantially higher than, the association rate constant is similar to, and the dissociation constant is substantially higher than those of the wild type. The three mutations, R82A, R92A, and V83GΔ84−89, decrease the rate constants for the chemical step by a factor of ~ 380, 3.5×10^4, and 1.1×10^5, respectively. The results suggest that neither R82 and R92 nor loop 3 is important for the binding of MgATP. R82 is dispensable for the binding of HP, R92 facilitates the binding of HP, and loop 3 helps to stabilize the HP-bound ternary complex. While R82 and R92 are important for the chemical step of pyrophosphoryl transfer, loop 3 is required to position these guanidinium groups into the catalytically competent positions and to seal the catalytic center assembly.

ACKNOWLEDGMENT

We thank Z. Dauter and K. R. Rajashankar for their help during X-ray diffraction data acquisition at the National Synchrotron Light Source, Brookhaven National Laboratory.

REFERENCES

1. Shiota, T. (1984) in *Chemistry and Biochemistry of Folates* (Blakley, R. T., and Benkovic, S. J., Eds.) pp 121−134, John Wiley & Sons, New York.
2. Blakley, R. L., and Benkovic, S. J. (1984) in *Folates and Pterins* (Blakley, R. L., and Benkovic, S. J., Eds.), John Wiley & Sons, New York.
3. Switzer, R. L. (1974) in *The Enzymes* (Boyer, P., Ed.) pp 607−629, Academic Press, New York.
4. Mildvan, A. S., Weber, D. J., and Abeygunawardana, C. (1999) *Adv. Enzymol. Relat. Areas Mol. Biol. 73*, 183−207.
5. Xiao, B., Shi, G., Chen, X., Yan, H., and Ji, X. (1999) *Structure (London) 7*, 489−496.
6. Hennig, M., Dale, G. E., D'Arcy, A., Danel, F., Fischer, S., Gray, C. P., Jolidon, S., Muller, F., Page, M. G., Pattison, P., and Oefner, C. (1999) *J. Mol. Biol. 287*, 211−219.
7. Stammers, D. K., Achari, A., Somers, D. O., Bryant, P. K., Rosemond, J., Scott, D. L., and Champness, J. N. (1999) *FEBS Lett. 456*, 49−53.
8. Blaszczyk, J., Shi, G., Yan, H., and Ji, X. (2000) *Structure (London) 8*, 1049−1058.
9. Li, Y., Gong, Y., Shi, G., Blaszczyk, J., Ji, X., and Yan, H. (2002) *Biochemistry 41*, 8777−8783.
10. Eriksen, T. A., Kadziola, A., Bentsen, A. K., Harlow, K. W., and Larsen, S. (2000) *Nat. Struct. Biol. 7*, 303−308.
11. Baker, L. J., Dorocke, J. A., Harris, R. A., and Timm, D. E. (2001) *Structure (London) 9*, 539−546.
12. Timm, D. E., Liu, J., Baker, L. J., and Harris, R. A. (2001) *J. Mol. Biol. 310*, 195−204.
13. Xiao, B., Shi, G., Gao, J., Blaszczyk, J., Liu, Q., Ji, X., and Yan, H. (2001) *J. Biol. Chem. 276*, 40274−40281.
14. Blaszczyk, J., Li, Y., Shi, G., Yan, H., and Ji, X. (2003) *Biochemistry 42*, 1573−1580.
15. Li, Y., Wu, Y., Blaszczyk, J., Ji, X., and Yan, H. (2003) *Biochemistry 42*, 1581−1588.
16. Thijssen, H. H. (1973) *Anal. Biochem. 54*, 609−611.
17. Scrimgeour, K. G. (1980) *Methods Enzymol. 66*, 517−523.
18. Shi, G., Gong, Y., Savchenko, A., Zeikus, J. G., Xiao, B., Ji, X., and Yan, H. (2000) *Biochim. Biophys. Acta 1478*, 289−299.
19. Kuzmic, P. (1996) *Anal. Biochem. 237*, 260−273.
20. Otwinowski, Z., and Minor, W. (1997) *Methods Enzymol. 276*, 307−326.
21. Navaza, J. (1994) *Acta Crystallogr., A 50*, 157−163.
22. Brünger, A. T., Adams, P. D., Clore, G. M., DeLano, W. L., Gros, P., Grosse-Kunstleve, R. W., Jiang, J. S., Kuszewski, J., Nilges, M., Pannu, N. S., Read, R. J., Rice, L. M., Simonson, T., and Warren, G. L. (1998) *Acta Crystallogr., D 54*, 905−921.
23. Sheldrick, G. M., and Schneider, T. R. (1997) *Methods Enzymol. 277*, 319−343.
24. Jones, T. A., and Kjeldgaard, M. (1997) *Methods Enzymol. 277*, 173−208.
25. Laskowski, R. A., MacArthur, M. W., Moss, D. S., and Thornton, J. M. (1993) *J. Appl. Crystallogr. 26*, 283−291.

26. Bermingham, A., Bottomley, J. R., Primrose, W. U., and Derrick, J. P. (2000) *J. Biol. Chem. 275*, 17962−12967.
27. Johnson, K. A. (1992) *The Enzymes*, pp 1−161, Academic Press, San Diego.
28. Esnouf, R. M. (1997) *J. Mol. Graphics Modell. 15*, 132−134, 112−113.
29. Merritt, E. A., and Bacon, D. J. (1997) *Methods Enzymol. 277*, 505−524.
30. Nicholls, A., Sharp, K. A., and Honig, B. (1991) *Proteins: Struct., Funct., Genet. 11*, 281−296.

BI036053L